

Article

Activity in the Photodegradation of 4-Nitrophenol of a Zn,Al Hydrotalcite-Like Solid and the Derived Alumina-Supported ZnO

Raquel Trujillano *, César Nájera and Vicente Rives * 

GIR-QUESCAT, Departamento de Química Inorgánica, Universidad de Salamanca, 37008 Salamanca, Spain; cesteban@usal.es

* Correspondence: rakel@usal.es (R.T.); vrives@usal.es (V.R.)

Received: 7 May 2020; Accepted: 19 June 2020; Published: 22 June 2020



Abstract: A Zn,Al layered double hydroxide (LDH), with the hydrotalcite structure and the mixed oxide obtained upon its calcination at 650 °C, was tested in the adsorption and photocatalytic degradation of 4-Nitrophenol in aqueous solution. The Zn,Al LDH was fast and easily obtained by the coprecipitation method. Hydrothermal treatment under microwave irradiation was applied to compare the effect of the ageing treatment on the photocatalytic behavior. The efficiency of the synthesized solids was compared to that of a commercial ZnO. The ageing treatment did not improve the performance of the original samples in the degradation of 4-nitrophenol. The activity of the synthesized solids tested exceeded that observed for the reaction with commercial ZnO. The photocatalytic performance of the original non-calcined hydrotalcite is similar to that of commercial ZnO. The calcined hydrotalcite showed a better performance in the adsorption-degradation of the contaminant than ZnO, and its reusability would be possible as it recovered the hydrotalcite-like structure during the reaction.

Keywords: photocatalysis; nitrophenol degradation; Zn,Al-hydrotalcite; ZnO dispersed on alumina; reusability; layered double hydroxide; LDH

1. Introduction

Although the use as photocatalysts of layered systems, and the mixed oxides derived from them by thermal decomposition, has been described in the literature, they are not as widely used as TiO₂. Discoloration of methylene blue using hydrotalcite-based catalysts was studied by Abderrazek et al. [1], while Barhoum et al. [2], among others, reported the photocatalytic activity of ZnO particles in the oxidation of methanol. More recently, Zhang et al. [3] synthesized nanostructured Zn-Al layered double hydroxides and have tested their photocatalytic activity, and that of the mixed oxides formed upon their calcination under different conditions, on the photodegradation of rhodamine dye in aqueous solutions.

Hydrotalcite is a layered hydroxycarbonate belonging to the so-called layered double hydroxides (LDHs) family, sometimes identified as anionic clays because of the similarity between their structure and that of clays, but with negative layers, electrically balanced by anions intercalated in the interlayers. These solids are transformed into well dispersed mixed oxides after being calcined at temperatures at or above 500 °C. Both the original materials and the derived oxides can act as catalysts or catalyst precursors in different industrially interesting reactions [3–7]. There are multiple synthesis routes to produce these solids [8–10]; among them, the co-precipitation method is the less expensive and the simplest one, and it is easily applied to manufacture this material at a large scale [11].

On the other hand, ZnO and modified ZnO have been widely studied in photocatalysis since the band gap energy of ZnO is similar to that of TiO₂ and it is cheaper than this one; deep and broad studies

about ZnO-based photocatalysts, their synthesis, reaction mechanisms and applications have been made available in recent years [12–14]. Lee et al. conclude that, in addition to its high photocatalytic activity, modification of ZnO photocatalysts is essential to improve its performance, especially in the field of organic dye degradation and, more specifically, in phenolic compounds removal [12].

There are also many papers about the use of LDHs as adsorbents for removal of phenolic contaminants [15]; the studies have pointed out the increase of the adsorption capacity of the mixed oxides when they are calcined at mild (below 700 °C) temperatures and recover the layered structure when they are suspended in a water solution containing anions (the potential contaminants in many cases), which are initially adsorbed on the solid nanoparticles to finally “rebuild” the original layered structure. This ability of hydrotalcites is called “memory effect” [16,17]. Chen et al. studied the kinetics of adsorption of phenol and 4-nitrophenol on Mg,Al-mixed oxides formed by thermal decomposition of a Mg,Al-LDH with the hydrotalcite structure [18]. These authors concluded that the adsorption mechanism involves the reconstruction by incorporating the nitrophenolate or phenolate ions in the interlayer and by adsorption on the surface.

4-nitrophenol (4-NP) is one of the most common contaminants in industrial waters, since it is used for the synthesis of drugs, fungicides, dyes, explosives, coloring agents for leather, etc., and it is also generated during formulation or degradation of some pesticides [19–22]. The aim of this work is to synthesize and characterize a Zn,Al-hydrotalcite with carbonate in the interlayer space, and to calcine it in order to obtain a Zn,Al mixed oxide to test both compounds in the photocatalytic degradation of 4-NP. Co-precipitation at constant pH is used to prepare the original layered sample [8] which, upon calcination, leads to a solid with a ZnO phase well dispersed in an amorphous Al₂O₃ phase; the synthesis procedure is the same as reported elsewhere [10]. The main interest of this work is in the study of the two possible ways of retention/degradation of these compounds, namely, adsorption and photocatalytic oxidation. The effect of microwave (MW) post-synthesis treatment of the original LDH is also studied. The performance of the materials prepared is compared to that of a commercial, unsupported ZnO.

2. Results and Discussion

2.1. Characterization of the Samples

Results from element chemical analysis for Zn and Al for both initial samples show the same content of zinc and aluminum (i.e., 50.28 and 6.45% (*w/w*), respectively). From these values, it is concluded that the composition was not affected by the microwave treatment applied to prepare sample ZnAlMW31, and taking into account the atomic masses of these cations, the real Zn/Al molar ratio is 3.17 (expected 3.00). FT-IR spectroscopy (see below) show that the only interlayer anion is carbonate, while thermogravimetric (TG) analysis data permitted to calculate the content of interlayer water, leading to the formula [Zn_{0.76}Al_{0.24}(OH)₂](CO₃)_{0.12}·0.71H₂O for both samples.

The Powder X-Ray Diffraction (PXRD) diagrams (Figure 1) for both the original, MW-treated and calcined samples show intense peaks in the characteristic positions of the hydrotalcite-like structure [10], corresponding to the rhombohedral hydrotalcite phase. The Miller indexes for the most significant signals are shown in the figure. Concerning the uncalcined samples, the peaks are better defined and are sharper and more symmetric for sample ZnAl31MW, evidencing its better crystallinity and layer stacking, probably as a result of the microwave post-synthesis treatment. Very weak peaks (not labelled in the figure) recorded in both diagrams are probably due to a very small portion of ZnO or Zn(OH)₂, which are preferentially segregated after the MW treatment.

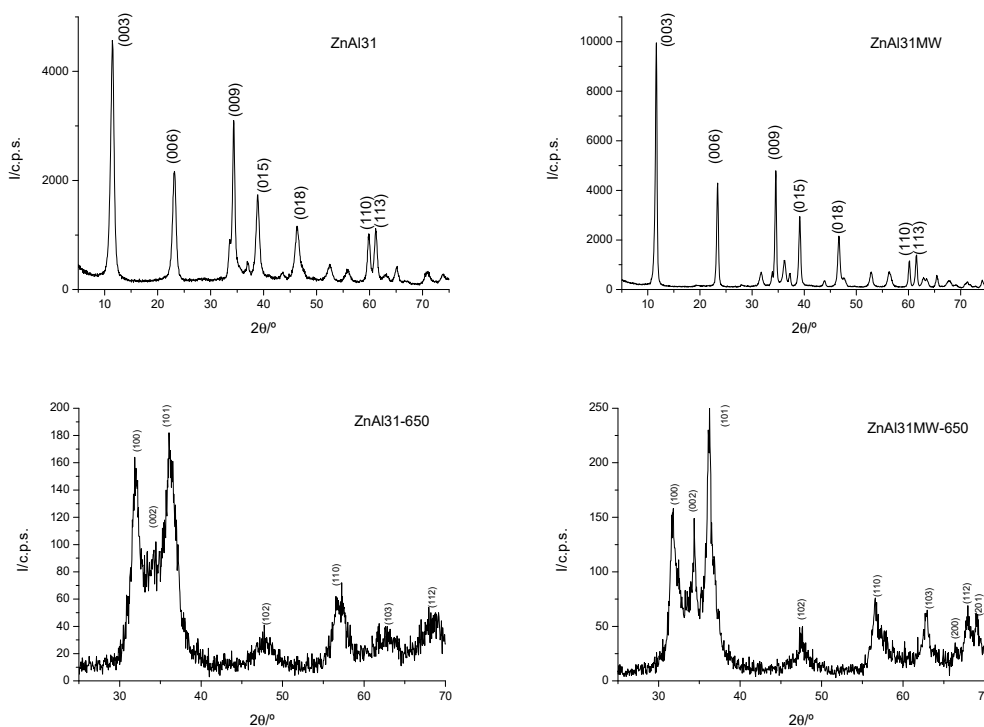


Figure 1. PXRD diagrams of: (**top**) Original samples (**left**) ZnAl31 and (**right**) ZnAl31MW, and (**bottom**) calcined samples (**left**) ZnAl31-650 and (**right**) ZnAl31MW-650. Ascription of the diffraction maxima to the corresponding planes, indicated by their Miller indexes, is shown.

Crystallographic data for these samples are included in Table 1, together with other data. Crystallographic parameters c and a were calculated from the positions of the diffraction peaks due to planes (003) and (110), respectively, assuming a rhombohedral phase; then, $c = 3 d(003)$ and $a = 2 d(110)$. The values are rather similar for both the original and the MW-treated samples, differences being only 1% for parameter c and ca. 0.3% for parameter a . The crystallite size values, also included in Table 1, were calculated by the Scherrer equation, from the full half-maximum width (FHMW, β) estimated by using commercial software Diffract Plus. Despite the crystallographic parameters are coincident within experimental error, the crystal size, both in the (003) and (110) directions (two directions were taken, due to the anisotropic nature of the material), is much greater for sample ZnAl31MW. The microwave hydrothermal treatment entails a much better crystallization, as it was observed by Benito et al. [10] for samples comparable to those here synthesized.

Table 1. Crystallographic parameters and crystallite sizes of the uncalcined samples.

Sample	c	a	β		D	
			(003)	(110)	(003)	(110)
ZnAl31	23.09	3.086	0.36	0.26	230	365
ZnAl31MW	22.85	3.074	0.17	0.19	480	510

β = full half-maximum width (FHMW) in $^\circ(2\theta)$; all other values in Å ; D rounded to $\pm 5 \text{ Å}$.

In order to check if the only anion in the interlayer balancing the positive layer charge in the uncalcined samples is carbonate, the FT-IR spectra of the samples were recorded; that for sample ZnAl31 is included in Figure 2. Several intense bands typical of hydrotalcite-like compounds [23] are recorded. The first one, centered around 3470 cm^{-1} , is due to the O-H stretching mode of the layer hydroxyl groups and interlayer water molecules. Broadening of this band toward the low wavenumber side indicates the existence of hydrogen bonds between the hydroxyl groups and carbonate anions [23,24]. The vibrational bending mode band of the interlayer water molecules is

observed at 1634 cm^{-1} , while the band at 1364 cm^{-1} is due to the ν_3 vibrational mode of interlayer carbonate species. The bands recorded below 800 cm^{-1} correspond to the stretching vibrations involving metal-hydroxyl, and metal-oxygen-metal bonds of the brucite layer cations [10,23,25,26]. No band due to intercalated nitrate (the counteranion of the Zn^{2+} and Al^{3+} salts used in the synthesis) is recorded.

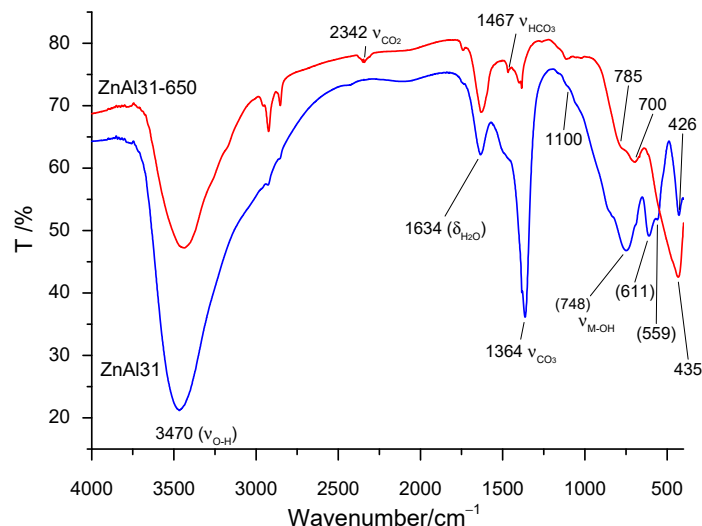


Figure 2. FT-IR spectra of samples ZnAl31 (blue line) and ZnAl31-650 (red line).

The results of the thermal analyses are included in Figure 3. The thermogravimetric (TG) curve shows a first mass loss amounting ca. 25% of the initial sample mass. The corresponding DTG (derivative thermogravimetric analysis) and DTA (differential thermal analysis) curves are also included in the same figure. The DTG curve is useful to identify the inflection points of the TG curve (where the mass loss rate reaches a maximum); in our case, these maxima are recorded at 160, 220 and 555 °C. The first two correspond also to the positions of the minima appearing in the DTA curve (the third minimum in the DTA curve is very poorly defined because of its extremely width), indicating that all these mass losses are due to endothermic processes. From mass spectrometric analysis of gases evolved during thermal decomposition of this type of solids [27], it was concluded that releasing of interlayer water molecules is responsible for the first mass loss, while further mass losses correspond to evolution of CO_2 (from interlayer carbonate species) and of H_2O , formed by condensation of layer hydroxyl groups. Another mass loss recorded between 300 and 650 °C, less than 10% of the initial sample mass, is related to a very broad and smooth endothermic effect in the DTA curve. This mass loss corresponds to the slow elimination of residual water and mainly CO_2 molecules [28], which migrate to the outside of the crystallites through the pores and channels (chimneys) generated during the previous intense dehydration–dehydroxylation–decarbonation processes. Elimination of these components results in the collapse of the structure, destroying the layered framework and forming an essentially amorphous phase that, when the temperature is further raised, leads to the formation of the spinel-type oxides, together with the oxide of the divalent cation [29].

Overall, the thermal decomposition of this sample follows the same trends as previously observed for other LDHs with easily decomposable interlayer species (e.g., carbonate or nitrate) and without oxidizable cations in the brucite-like layers [9,30]. From these results, we chose calcination at 650 °C as the calcination temperature to obtain well-dispersed ZnO , without segregation of new phases, to prepare new photocatalysts.

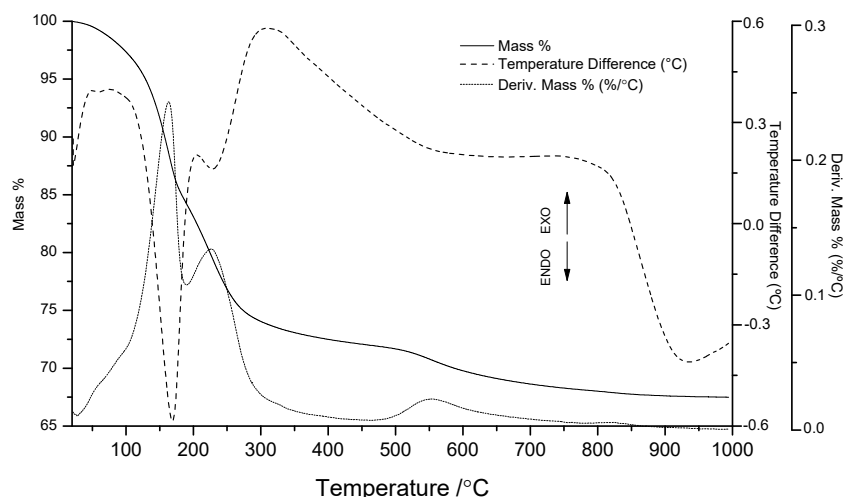


Figure 3. TG (solid), DTG (dotted) and DTA (dashed) curves of sample ZnAl31.

The PXRD diagrams for the calcined samples are included in Figure 1. The peaks of the LDH structure are no longer recorded, and the positions of the peaks are very close to those of ZnO, zincite (JCPDS standard n° 36-1451) [31].

The peaks are again better defined for sample ZnAl31MW-650, probably because of the higher crystallinity of the LDH precursor. The reflection planes (JCPDS 75-0576) are identified in the figure and correspond to the wurtzite-type structure [32–34]. No peaks corresponding to crystalline phases of Al oxides are recorded, meaning that, after calcination, aluminum remains forming amorphous phases, which might correspond to some sort of alumina, or even singly dispersed within the ZnO phase.

The FT-IR spectrum of sample ZnAl31-650 (Figure 2) confirms removal of interlayer anions upon calcination, as expected from the thermal analysis results, and confirming the collapse of the structure, as concluded from the PXRD results. On comparing the relative intensities of the bands due to water molecules bending and hydroxyl groups stretching modes, it is clear that in the calcined samples such bands are much weaker than in the uncalcined sample; at the same time, the bands due to the carbonate anion are completely (or almost completely) removed. Despite that carbonate has evolved as CO₂ during calcination, it is obvious that, due to the strong basic nature [35] of the oxides formed upon calcination, adsorption of atmospheric CO₂ and formation of surface carbonates species can be hardly avoided, thus it is not completely unexpected to record weak bands due to carbonate species in the spectra of calcined samples.

The band around 1365 cm⁻¹, the shoulder at 1467 cm⁻¹ and the weak feature at 1100 cm⁻¹ are due to vibrational modes of residual carbonate and probably hydrogencarbonate; the weak absorption close to 2342 cm⁻¹ is due to confined CO₂ molecules. The stability of these species is due to the strong basicity of this solid. The bands recorded around 785 and 700 cm⁻¹ are similar to the typical doublet due to the vibrations of “isolated” MO₄ tetrahedra at 785, 700 and 485 cm⁻¹, confirming the tetrahedral environment of the Zn²⁺ cations in the ZnO wurtzite-like phase [35].

Table 2 summarizes the surface texture data of these solids (two original samples with the LDH structure, and two calcined samples) concerning their surface areas: The Brunauer-Emmett-Teller (BET) specific surface data (S_{BET}), the external surface area (S_t) and the surface area equivalent to adsorption in micropores. First of all, the surface area equivalent to adsorption in micropores, S_{mp}, is rather low in all cases (even zero for sample ZnAl31, and around 10% in other cases), suggesting an insignificant presence of micropores. Secondly, the specific surface areas of the calcined samples are larger, in both cases, than for the corresponding uncalcined ones, in agreement with development of pores and channels as the escaping routes of internal species, water and CO₂ [36–39].

Table 2. Surface area data (m^2g^{-1}) for the samples studied *.

Sample	S_{BET}	S_{t}	S_{mp}
ZnAl31	51	51	0
ZnAl31MW	26	23	3
ZnAl31-650	73	66	7
ZnAl31MW-650	34	30	3

* S_{BET} : BET specific surface area; S_{t} = external surface area; S_{mp} = microporous-equivalent surface area.

A significant decrease in the specific surface area of the sample submitted to MW treatment, in comparison to that which had not been submitted to any post-synthesis treatment, is also observed. Actually, the specific surface area of sample ZnAl31MW is only one half of that for sample ZnAl31. This difference should be ascribed to the increase in the crystallinity of the sample after the MW treatment, as concluded from the larger sharpness and intensity of the PXRD peaks of sample ZnAl31MW compared to those of sample ZnAl31, as well as in the crystallite size, Table 1. Such a decrease in the specific surface area is “dragged” to the calcined samples: Although these have a larger specific surface area than the samples before calcination, the surface is still larger for the calcined sample prepared from the sample not submitted to the microwave hydrothermal treatment.

2.2. Degradation Studies

The catalytic activity of the samples in the photocatalytic degradation of 4-NP was measured; for this purpose, 750 mL of an aqueous solution with 25 ppm of 4-NP were introduced into the photoreactor and the catalyst was added to this solution. The amount of solid used in the degradation reactions was calculated in order to refer the measurements in all experiments to the activity of 200 ppm of Zn in different forms. The original solids, ZnAl31 and ZnAl31MW, were tested as catalysts and, in view of the results obtained therewith, one of the calcined sample, ZnAl31-650, was also tested. The activity of a commercial ZnO sample as a reference catalyst was also analyzed for comparison. The photolysis of the 4-nitrophenol solution, that is, the degradation of the contaminant under the action of ultraviolet light in the same experimental conditions, but in the absence of any catalyst, was studied as well. In all cases the solution (with or without dispersed catalyst) was continuously stirred and small volumes (aliquots) were taken periodically in order to follow the reaction by UV-Vis spectroscopy, by monitoring the decrease in the intensity of the typical band of 4-NP at 400 nm.

To study the adsorption, the suspension is stirred in the reaction chamber and kept in the darkness until a constant concentration of the contaminant was reached; at that time the suspension is irradiated with ultraviolet light to study the photocatalytic reaction.

When the catalyst is added to the solution, 4-nitrophenol is deprotonated due to the basicity of these solids and the band typical of the phenolate group at 400 nm is recorded [40,41]. For this reason, the degradation of the contaminant was studied taking, as a reference, the maximum absorbance of this band and following its decrease as the reaction time elapses.

The results obtained for the adsorption of 4-NP in the absence of light using ZnAl31 and ZnAl31MW are shown in Figure 4; those obtained in the same conditions with a commercial ZnO are included for comparison.

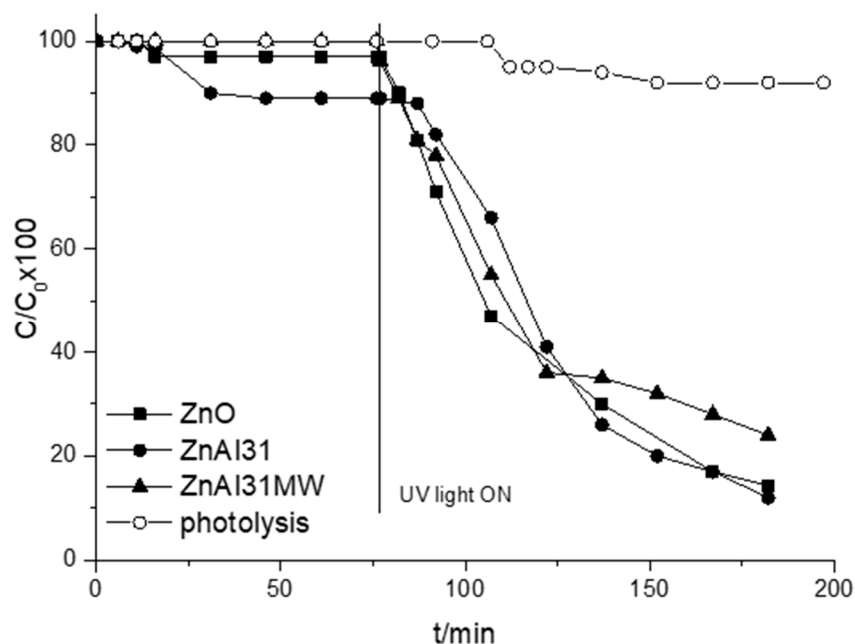


Figure 4. 4-NP degradation using ZnAl31, ZnAl31MW and commercial ZnO. Photolysis (open circles) is included for comparison.

The decrease in the contaminant concentration in the darkness is probably due to its adsorption or absorption on the catalyst used. It can be concluded that in the darkness there is no significant adsorption on sample ZnAl31MW. However, the relative concentration of the contaminant decreases by about 3 and 10%, respectively, on samples ZnO and ZnAl31 after 30 min and remains constant for longer times. This decrease is probably due to the adsorption of the contaminant on the surface of the solids, and it should be noticed that it is greater on sample ZnAl31, perhaps because of its larger specific surface area and also because, in this case, part of the contaminant can enter the interlayer space. On the contrary, the curve for sample ZnAl31MW shows that the adsorption of the contaminant is constant and almost negligible during all time tested.

After 75 min in the darkness the reaction was continued under UV light, in order to check the photocatalytic activity of the solids. After 40 min of illumination, between 40 and 50% of the initial 4-NP was degraded and after 50 min the amount of 4-NP degraded is the same for all samples. When the reaction time is further extended, the degradation practically stabilizes for sample ZnAl31MW and increases slightly for ZnO and ZnAl31, both curves becoming almost coincident when the reaction time is further prolonged. In other words, the experimental results indicate that the MW ageing treatment to which the ZnAl31MW sample was submitted does not improve its photocatalytic activity if compared to that of ZnAl31, which matched the degradation capacity of ZnO. For this reason, the study was continued only with the calcined sample, ZnAl31-650, prepared from sample ZnAl31.

The degradation curve obtained in the darkness using sample ZnAl31-650 is shown in Figure 5, together with that for ZnO. It is worth noting that for sample ZnAl31-650 the adsorption reaches 54% after 45 min and 67% after 75 min and then stabilizes. When the reaction continues under UV light, removal of 4-NP after 30 min reaches 75% for sample ZnAl31-650, while it is 53% for pure ZnO, and after 60 min it is 90% for sample ZnAl31-650 and only 70% for sample ZnAl31 or ZnO.

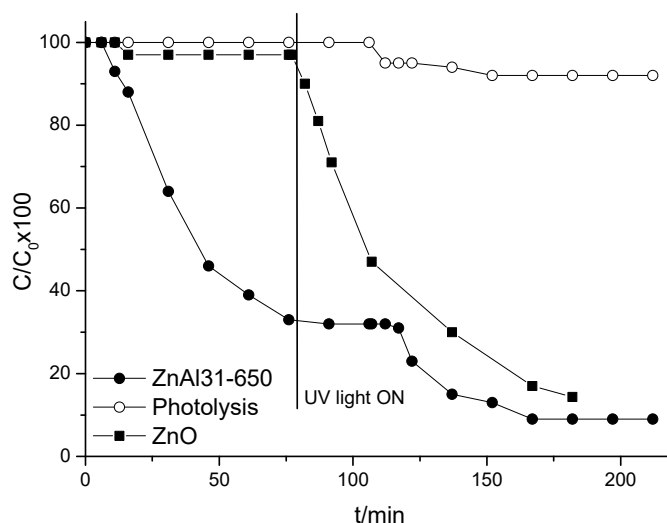


Figure 5. 4-NP degradation using ZnAl31-650 and ZnO. Photolysis (open circles) results are included for comparison.

In order to confirm the photocatalytic capacity of sample ZnAl31-650, some aliquots of solution were withdrawn from the reaction medium at different reaction times (in the darkness and under UV light) and analyzed by mass spectrometry. Aliquot D5 was withdrawn after 5 min in the darkness, while aliquots L10, L30 and L165 were withdrawn after 10, 30 and 165 min under UV light, respectively.

The mass spectrum of the solution collected after 5 min of reaction in the darkness (Supplementary material, Figure S1), D5, shows a weak signal at about m/z 139 corresponding to a small portion of the nitrophenol molecule together with an intense signal recorded at m/z close to 138, with intensity 1.4×10^7 (in arbitrary units) which would correspond to deprotonated 4-nitrophenol. This deprotonation is not unexpected, since the catalyst provides a basic character to the solution of the contaminant and in this medium 4-NP (molecular mass 139.1) loses the proton of the alcohol function being transformed into the nitrophenolate anion (mass 138.1), as already confirmed by the analysis of the absorption spectra previously discussed. A very weak signal recorded at m/z 168 may be due to the combination of fragments formed in the mass spectrometer chamber. These results confirm that in the darkness there is no degradation of 4-nitrophenol and only adsorption/absorption can occur on the catalyst surface. The signal at m/z 108 (less than 0.1×10^7 of relative intensity) indicates that diquinone begins to form in the reactor, the first by-product that suggests the incipient oxidation of the substrate that will accelerate when the ultraviolet light strikes the reaction medium.

In the mass spectrum of aliquot L10 (Supplementary material, Figure S2), it is noteworthy that the decrease in the intensity in the signal due to the molecular fragment of the contaminant, which decreases from ca. 1.5×10^7 for sample D5, to 6×10^6 for sample L10, that is, after 10 min of reaction under UV light. In this spectrum, very weak signals are recorded at m/z 124.9, 174.7 and 201.1, which may correspond to the hydroxybenzoquinone molecule, and to fragments formed by aggregates of by-products during the reaction or in the mass spectrometer chamber. These data indicate that after 10 min of UV irradiation, by-products of the oxidation of 4-nitrophenol are already formed [42,43].

In the mass spectrum of aliquot L30 (Supplementary material, Figure S3), the previously described signals are again recorded, in addition to another one at m/z 153.9. According to results reported in the literature [42], this signal could be due to deprotonated 4-nitrocatechol, which is formed during degradation by hydroxylation prior to the oxidation of the contaminant.

The mass spectrum of the last aliquot collected (Supplementary material, Figure S4) confirms that the concentration of the pollutant molecule is practically null and the spectrum shows signals of reaction by-products or aggregates thereof. These signals indicate that after this reaction time the oxidation of the contaminant was completed.

Figure 6 shows the evolution of the intensity of the molecular signal of the contaminant ($m/z = 137.9$) with the reaction time in the aliquots analyzed by mass spectrometry. As it can be seen, at the end of the reaction this signal has completely disappeared, that is, after 165 min of photocatalytic reaction 4-NP was completely degraded.

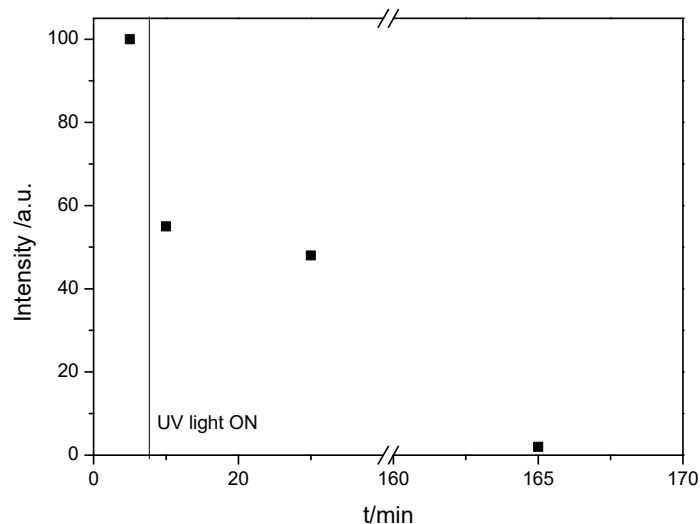


Figure 6. Evolution of the relative intensity of the m/z 137.9 signal for the aliquots analyzed by mass spectrometry. Dots (from left to right) correspond to aliquots D5, L10, L30 and L165, respectively.

In order to study the possible reusability of the catalyst, sample ZnAl31-650 was collected and dried after the whole experiment (reaction in the darkness and under UV light) to study the structural changes undergone by the catalyst during the reaction (the sample was named as ZnAl31-650Rec). The PXRD diagram of this sample reveals that the layered structure of the original hydrotalcite is, in a large extent, recovered during the reaction and reveals the possibility of reusing it after a new calcination cycle. Figure 7 shows the PXRD diagrams of the calcined (before photocatalytic tests) and recovered samples, and the inset includes a comparison of the diagram of the original hydrotalcite (ZnAl31) with that of the recovered catalyst, ZnAl31-650Rec. These results undoubtedly demonstrate that the catalysts could be reusable.

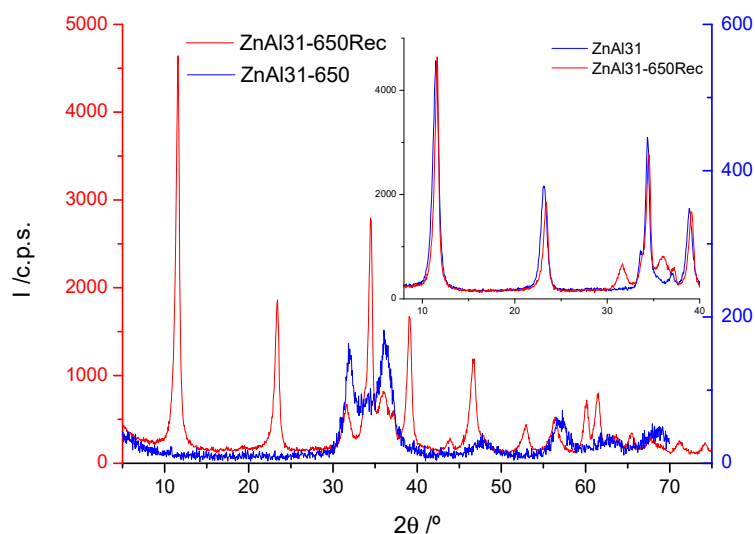


Figure 7. PXRD diagrams of samples ZnAl31-650Rec and ZnAl31-650. Inset: ZnAl31-650Rec and ZnAl31 samples.

The FT-IR spectrum of sample ZnAl31-650Rec (Figure 8) was recorded in order to confirm the reconstruction of the layered structure after the reaction and also to determine if bands belonging to the contaminant molecule are present. The spectra of samples ZnAl31 and ZnAl31-650 were included in the figure for comparison. It is remarkable that after the reaction the sample shows an FT-IR spectrum similar to that of the original, uncalcined sample. The increase in intensity of the carbonate band of the ZnAl31-650Rec compared to that for ZnAl31-650 indicates that the sample has absorbed this anion (probably formed upon complete degradation of 4-NP) to reconstruct the layered structure.

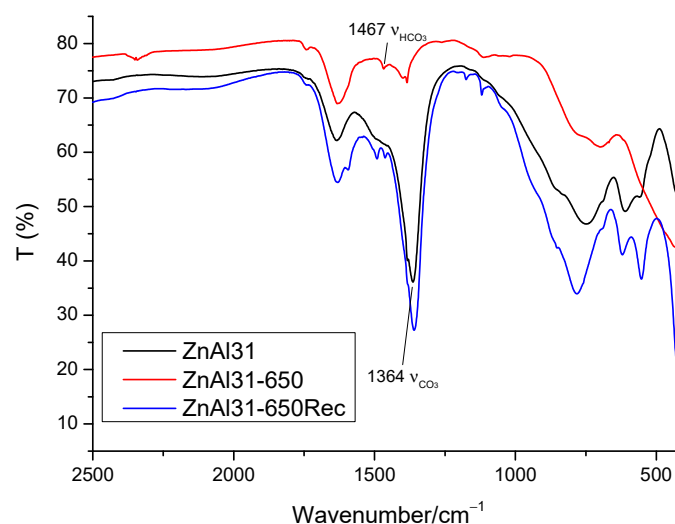


Figure 8. FT-IR spectra of samples ZnAl31-650Rec, ZnAl31 and ZnAl31-650.

3. Materials and Methods

All inorganic reagents, zinc nitrate hexahydrate (98%), aluminum nitrate nonahydrate (98%), zinc oxide (99.9%), sodium carbonate, sodium hydroxide and potassium bromide (analytical purity) were supplied by PanReac AppliChem (Castellar del Vallés, Barcelona, Spain); 4-nitrophenol was purchased to Merck KGaA (Darmstadt, Germany) and liquid nitrogen and gases used for analysis (N_2 , O_2 , and He) were supplied by L’Air Liquide, S. A. (Madrid, Spain).

The Zn,Al hydrotalcite with carbonate in the interlayer was synthesized by slowly adding an aqueous solution of the cation salts (0.5 M Zn^{2+} and 0.165 M Al^{3+}) with a Zn:Al molar ratio of 3:1 to a 0.11 M solution of sodium carbonate (CO_3^{2-}/Al^{3+} molar ratio = 1); the pH of the mixture was kept constant at 10 by adding 1 M NaOH using a pH-burette 24 from Crison. Once the addition was complete, a portion of the suspension was kept under stirring in air for 24 h and the other one was submitted to hydrothermal treatment in a microwave oven (Milestone Ethos Plus) at 100 °C for 2 h. Both suspensions obtained were centrifuged and the solids were washed with distilled water to remove the counterions (nitrate and sodium). Then, they were dried at room temperature in open air and hand ground in an agate mortar. The samples thus obtained were named as ZnAl31 and ZnAl31MW, respectively, where “MW” stands for microwave (MW) treatment. Both samples were calcined at 650 °C (leading to samples named ZnAl31-650 and ZnAl31MW-650, respectively) in order to obtain mixtures of well dispersed oxides. This calcination temperature was selected after recording the thermogravimetric analysis of the original samples.

The samples were characterized by the techniques described below. Element chemical analyses were performed by atomic absorption in a Perkin Elmer Elan 6000 ICP Mass Spectra apparatus at Servicio General de Análisis Químico Aplicado (Universidad de Salamanca, Spain). The powder X-ray diffraction (PXRD) analysis was carried out using a Siemens D-5000 diffractometer, with an electric power of 1200 W (30 mA and 40 kV), 0.05 °/step and 1.5 s/step (scanning rate 2 °/min). The FT-IR spectra were recorded using the KBr pressed pellet method in a Perkin-Elmer Spectrum-One spectrometer, with a nominal resolution of 4 cm^{-1} and averaging 50 scans to improve the signal-to-noise

ratio. Specific surface area measurement and porosity analysis were carried out from the nitrogen adsorption-desorption isotherms at $-196\text{ }^{\circ}\text{C}$. The isotherms were recorded in a Micromeritics Gemini VII 2390t equipment. Before analysis the samples were treated under dry nitrogen flow for 2 h at $110\text{ }^{\circ}\text{C}$ in a Micromeritics FlowPrep 060 Sample Degass System apparatus to remove weakly adsorbed species. Thermogravimetric and differential thermal analyses (TGA and DTA) were recorded from room temperature to $1000\text{ }^{\circ}\text{C}$ at a heating rate of $10\text{ }^{\circ}\text{C}/\text{min}$ under a continuous oxygen flow in an SDT Q600 apparatus from TA INSTRUMENTS.

A MPDS-Basic system from Peschl Ultraviolet, with a PhotoLAB Batch-L reactor and a TQ150-Z0 lamp (power 150 W), integrated in a photonCABINET was used to check the photoactivity. Its spectrum is continuous, with the main peaks at 366 nm (radiation flux, ϕ 6.4 W) and 313 nm (ϕ 4.3 W). The solutions were analyzed by ultraviolet-visible spectroscopy in order to control the progress of the reaction in a Perkin-Elmer LAMBDA 35 spectrophotometer coupled to a computer with UV WINLAB 2.85 software.

Aiming to determine the by-products generated during UV degradation, some selected solutions were analyzed after various reaction times by mass spectrometry. The equipment used was an Agilent 1100 HPLC mass spectrometer coupled to an ultraviolet detector and an Agilent Trap XCT mass spectrometer. These analyses were carried out at Servicio Central de Análisis Elemental, Cromatografía y Masas (Universidad de Salamanca, Spain).

4. Conclusions

The synthesis method used without further treatment facilitates a rapid and effective production of the original solid, ZnAl31, whose calcination at $650\text{ }^{\circ}\text{C}$ allows obtaining a solid with higher specific surface area and consisting of a ZnO phase dispersed on an Al_2O_3 amorphous phase.

The activity of the synthesized solids tested for the degradation reaction of 4-nitrophenol in aqueous solution exceeded that observed for the reaction with a commercial ZnO. The photocatalytic performance of the original non-calcined hydrotalcite is similar to that of commercial ZnO. The ZnAl31-650 sample shows the best performance in the adsorption-degradation of the contaminant, perhaps because of its high specific surface area and the high dispersion of the active phase. These two characteristics are a consequence of the use of a synthetic hydrotalcite as the ZnO active phase precursor, thus the final solid acts by adding its capacity as a photocatalyst to its capacity as an adsorbent.

Supplementary Materials: The following are available online at <http://www.mdpi.com/2073-4344/10/6/702/s1>, Figure S1: Mass spectrum of aliquot D5, after 5 min in the darkness, Figure S2: Mass spectrum of aliquot L10, after 10 min under UV light, Figure S3: Mass spectrum of aliquot L30, after 30 min under UV light, Figure S4: Mass spectrum of aliquot L165, after 165 min under UV light.

Author Contributions: Conceptualization, methodology and validation V.R. and R.T.; investigation C.N., resources V.R. and R.T.; original draft, C.N.; supervision, R.T. and V.R. All authors have read and agreed to the published version of the manuscript reported.

Funding: The project leading to this submission received funding from MAT2016-78863-C2-2-R.

Conflicts of Interest: The authors declare no conflicts of interest.

References

1. Abderrazek, K.; Najoua, F.S.; Srasra, S. Synthesis and characterization of [Zn–Al] LDH: Study of the effect of calcination on the photocatalytic activity. *Appl. Clay Sci.* **2016**, *119*, 229–235. [[CrossRef](#)]
2. Barhoum, A.; Melcher, J.; Van Assche, G.; Rahier, H.; Bechelany, M.; Fleisch, M.; Bahnemann, D. Synthesis, growth mechanism, and photocatalytic activity of Zinc oxide nanostructures: Porous microparticles versus nonporous nanoparticles. *J. Mater. Sci.* **2017**, *52*, 2746–2762. [[CrossRef](#)]
3. Zhang, Z.; Hua, Z.; Lang, J.; Song, Y.; Zhang, Q.; Han, Q.; Fan, H.; Gao, M.; Li, X.N.; Yang, J. Eco-friendly nanostructured Zn–Al layered doublehydroxide photocatalysts with enhanced photocatalytic activity. *Cryst. Eng. Commun.* **2019**, *21*, 4607–4619. [[CrossRef](#)]

4. Basile, F.; Benito, P.; Fornasari, G.; Rosetti, V.; Scavetta, E.; Tonelli, D.; Vaccari, A. Electrochemical synthesis of novel structured catalysts for H₂ production. *Appl. Catal. B Environ.* **2009**, *91*, 563–572. [[CrossRef](#)]
5. Chai, R.; Li, Y.; Zhang, Q.; Fan, S.; Zhang, Z.; Chen, P.; Zhao, G.; Liu, Y.; Lu, Y. Foam-Structured NiO-MgO-Al₂O₃ Nanocomposites Derived from NiMgAl Layered Double Hydroxides In Situ Grown onto Nickel Foam: A Promising Catalyst for High-Throughput Catalytic Oxymethane Reforming. *Chem. Catal. Chem.* **2017**, *9*, 268–272.
6. Chai, R.; Fan, S.; Zhang, Z.; Chen, P.; Zhao, G.; Liu, Y.; Lu, Y. Free-Standing NiO-MgO-Al₂O₃ Nanosheets Derived from Layered Double Hydroxides Grown onto FeCrAl-Fiber as Structured Catalysts for Dry Reforming of Methane. *ACS Sustain. Chem. Eng.* **2017**, *5*, 4517–4522. [[CrossRef](#)]
7. Chai, R.; Zhang, Z.; Chen, P.; Zhao, G.; Liu, Y.; Lu, Y. Ni-foam-structured NiO-MOx-Al₂O₃ (M = Ce or Mg) nanocomposite catalyst for high throughput catalytic partial oxidation of methane to syngas. *Microporous Mesoporous Mater.* **2017**, *253*, 123–128. [[CrossRef](#)]
8. Rives, V. (Ed.) *Layered Double Hydroxides: Present and Future*; Nova Science Publishers: New York, NY, USA, 2001.
9. Trujillano, R.; González-García, I.; Morato, A.; Rives, V. Controlling the Synthesis Conditions for Tuning the Properties of Hydrotalcite-Like Materials at the Nano Scale. *ChemEngineering* **2018**, *2*, 31. [[CrossRef](#)]
10. Benito, P.; Guinea, I.; Labajos, F.M.; Rocha, J.; Rives, V. Microwave-hydrothermally aged Zn,Al hydrotalcite-like compounds: Influence of the composition and the irradiation conditions. *Micropor. Mesopor. Mat.* **2008**, *110*, 292–302. [[CrossRef](#)]
11. Mishraa, G.; Dasha, B.; Pandey, S. Layered double hydroxides: A brief review from fundamentals to application as evolving biomaterials. *Appl. Clay Sci.* **2018**, *153*, 172–186. [[CrossRef](#)]
12. Lee, K.M.; Lai, C.W.; Ngai, K.S.; Juan, J.C. Recent developments of zinc oxide based photocatalyst in water treatment technology: A review. *Water Res.* **2016**, *88*, 428–448. [[CrossRef](#)] [[PubMed](#)]
13. Ong, C.B.; Ng, L.Y.; Abdul, W.M. A review of ZnO nanoparticles as solar photocatalysts: Synthesis, mechanisms and applications. *Renew. Sustain. Energy Rev.* **2018**, *81*, 536–551. [[CrossRef](#)]
14. Serrà, A.; Zhang, Y.; Sepúlveda, B.; Gómez, E.; Nogués, J.; Michler, J.; Philippe, L. Highly active ZnO-based biomimetic fern-like microleaves for photocatalytic water decontamination using sunlight. *Appl. Catal. B Environ.* **2019**, *248*, 129–146. [[CrossRef](#)]
15. He, X.; Wang, B.; Zhang, Q. Phenols removal from water by precursor preparation for MgAl layered double hydroxide: Isotherm, kinetic and mechanism. *Mater. Chem. Phys.* **2019**, *221*, 108–117. [[CrossRef](#)]
16. Kwon, T.; Pinnavaia, T.J. Pillaring of a layered double hydroxide by polyoxometalate with Keggin-ion structures. *Chem. Mater.* **1989**, *14*, 381–383. [[CrossRef](#)]
17. Chibwe, K.; Jones, W. Intercalation of organic and inorganic anions into layered hydroxides. *J. Chem. Soc. Chem. Commun.* **1989**, *14*, 926–927. [[CrossRef](#)]
18. Chen, S.; Xu, Z.P.; Zhang, Q.; Lu, G.Q.M.; Hao, Z.P.; Liu, S. Studies on adsorption of phenol and 4-nitrophenol on MgAl-mixed oxide, derived from MgAl layered double hydroxides. *Sep. Pur. Technol.* **2009**, *67*, 194–200. [[CrossRef](#)]
19. Rajamanickam, D.; Shanthi, M. Photocatalytic degradation of an organic pollutant by zinc oxide—Solar process. *Arab. J. Chem.* **2016**, *9*, S1858–S1868. [[CrossRef](#)]
20. Zheng, Y.; Shu, J.; Wang, Z. AgCl@Ag composites with rough surfaces as bifunctional catalyst for the photooxidation and catalytic reduction of 4-nitrophenol. *Mater. Lett.* **2015**, *158*, 339–342. [[CrossRef](#)]
21. Uberoi, V.; Bhattacharya, S.K. Toxicity and degradability of nitrophenols in anaerobic systems. *Water Environ. Res.* **1997**, *69*, 146–156. [[CrossRef](#)]
22. Kidak, R.; Ince, N.H. Ultrasonic destruction of phenol and substituted phenols: A review of current research. *Ultrason. Sonochem.* **2006**, *13*, 195–199. [[CrossRef](#)]
23. Klopogge, J.T.; Frost, R.L. Infrared and Raman Spectroscopic Studies of Layered Double Hydroxides (LDHs). In *Layered Double Hydroxides: Present and Future*; Rives, V., Ed.; Nova Science Publisher: New York, NY, USA, 2001; Chapter 5; pp. 139–192.
24. Klopogge, T.; Hickey, L.; Frost, R. FT-Raman and FT-IR spectroscopic study of synthetic Mg/Zn/Al hydrotalcites. *J. Raman Spectrosc.* **2004**, *35*, 967–974. [[CrossRef](#)]
25. Alzamora, L.E.; Ross, J.R.H.; Kruissink, E.C.; Van Reijden, L.L. Coprecipitated nickel–alumina catalysts for methanation at high temperature. Part 2—Variation of total and metallic areas as a function of sample composition and method of pretreatment. *J. Chem. Soc. Faraday Trans. I* **1981**, *77*, 665. [[CrossRef](#)]

26. Klopogge, J.T. Infrared and Raman spectroscopy of naturally occurring hydrotalcites and their synthetic equivalents. In *The Application of Vibrational Spectroscopy to Clay Minerals and Layered Double Hydroxides*; Klopogge, J.T., Ed.; CMS Workshop Lectures; The Clay Minerals Society: Aurora, CO, USA, 2005; Volume 13, pp. 203–238.
27. Rives, V. Comment on “Direct Observation of a Metastable Solid Phase of Mg/Al/CO₃-Layered Double Hydroxide by Means of High-Temperature in Situ Powder XRD and DTA/TG”. *Inorg. Chem.* **1999**, *38*, 406–407. [[CrossRef](#)]
28. Miyata, S. Anion-exchange properties of hydrotalcite-like compounds. *Clays Clay Min.* **1983**, *31*, 305. [[CrossRef](#)]
29. Labajos, F.M.; Rives, V.; Ulibarri, M.A. Effect of hydrothermal and thermal treatments on the physicochemical properties of Mg-Al hydrotalcite-like materials. *J. Mater. Sci.* **1992**, *27*, 1546–1552. [[CrossRef](#)]
30. Rives, V. Study of Layered Double Hydroxides by Thermal Methods. In *Layered Double Hydroxides: Present and Future*; Rives, V., Ed.; Nova Science Publishers: New York, NY, USA, 2001; Chapter 4; pp. 115–137, ISBN 1-59033-060-9.
31. Basnet, P.; Samanta, D.; Inakhunbi Chanu, T.; Mukherjee, J.; Chatterjee, S. Assessment of synthesis approaches for tuning the photocatalytic property of ZnO nanoparticles. *SN Appl. Sci.* **2019**, *1*, 633. [[CrossRef](#)]
32. Amari, R.; Mahroug, A.; Boukhari, A.; Deghfel, B.; Selmi, N. Structural, Optical and Luminescence Properties of ZnO Thin Films Prepared by Sol-Gel Spin-Coating Method: Effect of Precursor Concentration. *Chin. Phys. Lett.* **2018**, *35*, 016801. [[CrossRef](#)]
33. Prasada Rao, T.; Santhoshkumar, M.C. Effect of thickness on structural, optical and electrical properties of nanostructured ZnO thin films by spray pyrolysis. *Appl. Surf. Sci.* **2009**, *255*, 4579–4584. [[CrossRef](#)]
34. Wang, L.; Lou, Z.; Fei, T.; Zhang, T. Templating synthesis of ZnO hollow nanospheres loaded with Au nanoparticles and their enhanced gas sensing properties. *J. Mater. Chem.* **2012**, *22*, 4767–4771. [[CrossRef](#)]
35. Montanari, T.; Sisani, M.; Nocchetti, M.; Vivani, R.; Herrera Delgado, M.C.; Ramis, G.; Busca, G.; Costantino, U. Zinc-aluminum hydrotalcites as precursors of basic catalysts: Preparation, characterization and study of the activation of methanol. *Catal. Today* **2010**, *152*, 104–109. [[CrossRef](#)]
36. Carriazo, D.; del Arco, M.; García-López, E.; Marci, G.; Martín, C.; Palmisano, L.; Rives, V. Zn,Al hydrotalcites calcined at different temperatures: Preparation, characterization and photocatalytic activity in gas-solid regime. *J. Mol. Catal. A Chem.* **2011**, *342–343*, 83–90. [[CrossRef](#)]
37. Rives, V. Characterization of layered double hydroxides and their decomposition products. *Mater. Chem. Phys.* **2002**, *75*, 19–25. [[CrossRef](#)]
38. Rives, V. Surface Texture and Electron Microscopy Studies of Layered Double Hydroxides. In *Layered Double Hydroxides: Present and Future*; Nova Science Publishers: New York, NY, USA, 2001; Chapter 8; pp. 229–250.
39. Reichle, W.T.; Kang, S.Y.; Everhardt, D.S. The nature of the thermal decomposition of a catalytically active anionic clay mineral. *J. Catal.* **1986**, *101*, 352. [[CrossRef](#)]
40. Mancipe, S.; Tzompantzi, F.; Rojas, H. Photocatalytic degradation of phenol using MgAlSn. *Appl. Clay Sci.* **2016**, *129*, 71–78. [[CrossRef](#)]
41. Mancipe, S.; Tzompantzi, F.; Gómez, R. Photocatalytic reduction of 4-nitrophenol to 4-aminophenol over CdS/MgAl layered double hydroxide catalysts under UV irradiation. *React. Kinet. Mech. Catal.* **2017**, *122*, 625–634. [[CrossRef](#)]
42. Anuradha, G.; Meenukhurana Archana, C.; Masahiro, T.; Asit, K.C.; Rakesh, K.J. Degradation of 4-Nitrophenol, 2-Chloro-4-nitrophenol, and 2,4-dinitrophenol. *Environ. Sci. Technol.* **2010**, *44*, 1069–1077.
43. Wei, L.; Zhu, H.; Mao, X.; Gan, F. Electrochemical oxidation process combined with UV photolysis for the mineralization of nitrophenol in saline wastewater. *Sep. Purif. Technol.* **2011**, *77*, 18–25. [[CrossRef](#)]

